Nanosized carriers based on amphiphilic poly-N-vinyl-2-pyrrolidone for intranuclear drug delivery

Luss, Anna L; Kulikov, Pavel P; Romme, Sven B; Andersen, Camilla L; Pennisi, Cristian P; Docea, Anca O; Kuskov, Andrey N; Velonia, Kelly; Mezhuev, Yaroslav O; Shtilman, Mikhail I; Tsatsakis, Aristidis M; Gurevich, Leonid

Published in:
Nanomedicine

DOI (link to publication from Publisher):
10.2217/nnm-2017-0311

Publication date:
2018

Document Version
Publisher's PDF, also known as Version of record

Research Article

For reprint orders, please contact: reprints@futuremedicine.com

Nanomedicine

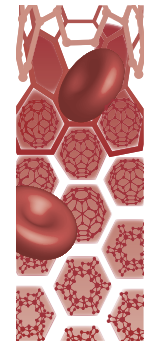

Nanosized carriers based on amphiphilic poly-N-vinyl-2-pyrrolidone for intranuclear drug delivery

Anna L Luss[1], Pavel P Kulikov[1], Sven B Romme[2], Camilla L Andersen[2], Cristian P Pennisi[3], Anca O Docea[4], Andrey N Kuskov[1], Kelly Velonia*[,5], Yaroslav O Mezhuev[1], Mikhail I Shtilman[1,7], Aristidis M Tsatsakis**[,6,7] & Leonid Gurevich***[,2]

[1]Department of Biomaterials, Dmitry Mendeleev University of Chemical Technology of Russia, Miusskaya sq 9, 125047 Moscow, Russia

[2]Department of Materials & Production, Aalborg University, Skjernvej 4A, 9220, Aalborg, Denmark

[3]Department of Health Science & Technology, Aalborg University, Fredrik Bajers Vej 3, 9220, Aalborg, Denmark

[4]Department of Toxicology, Faculty of Pharmacy, University of Medicine & Pharmacy, 2 Petru Rares, 200349, Craiova, Romania

[5]Department of Materials Science & Technology, School of Sciences & Engineering, University of Crete, University Campus Voutes, 71003 Heraklion, Crete, Greece

[6]Laboratory of Toxicology, Medical School, University of Crete, Voutes, Heraklion Crete 71003, Greece

[7]Bauman Moscow State Technical University, Center Composites of Russia, 2nd Baumanskaya 5, 105005 Moscow, Russia

*Author for correspondence: velonia@materials.uoc.gr

**Author for correspondence: tsatsaka@uoc.gr

***Author for correspondence: lg@nano.aau.dk

Aim: Ability to deliver drugs into the cell nuclei can significantly increase the efficacy of cancer therapies, in particular in the case of multidrug-resistant cancer **Results:** Polymer nanocarriers based on amphiphilic thiooctadecyl-terminated poly-N-vinyl-2-pyrrolidone were produced and loaded with a model hydrophobic drug, curcumin. Two commonly used loading approaches – emulsification and ultrasonic dispersion – were found to lead to two different size distributions with distinctively different biological effect. While nanocarriers produced via the emulsion method penetrated cells by dynamin-dependent endocytic mechanisms, sub-100 nm dispersion-produced nanocarriers were capable of crossing the membranes via biologically independent mechanisms. **Conclusion:** This finding opens an intriguing possibility of intranuclear delivery by merely tailoring the size of polymeric carriers, thus promising a new approach for cancer therapies.

First draft submitted: 5 October 2017; Accepted for publication: 23 January 2018; Published online: 4 May 2018

Keywords: atomic force microscopy • curcumin • fluorescence microscopy • intranuclear drug delivery • nanocarrier • PVP

Nanoformulated drug-delivery systems based on various nanoncarriers – liposomes, micelles, nanoparticles, etc. – are rapidly becoming the mainstream approach in medicine, in particular, cancer therapy. They offer a number of advantages compared with systemical application of drugs, including prolonged circulation time, ability of cell-specific targeting through passive and active mechanisms, and controlled drug release [1]. As a result, nanocarriers protect their cargo from degradation, increase the efficacy of drugs and reduce toxicity to healthy tissue and hence unwanted side effects. Since most of the anticancer drugs attack cell DNA, the ability to penetrate cell nuclei can significantly increase the therapeutic efficacy. This becomes particularly important for treatment of multidrug-resistant cancer, since low molecular drug released in cytoplasm can be still cleared of the multidrug-resistant cells [2].

Cellular uptake of nanoparticle carriers usually occurs through endocytic pathways [3,4]. Briefly, a particle that comes into contact with the cell exterior becomes engulfed by the cell membrane, forming an invagination, which afterward separates from the membrane as a vesicle and transports its cargo to various intracellular destinations. Most of the time, particles are treated by the cell as foreign objects and transported to lysosomes causing degradation

Future Medicine

and loss of activity [5,6]. In this respect, the uptake of nanoparticle carriers [7–9] containing pharmaceutically active substances by cells through different mechanisms is of considerable interest as it can ensure delivery of therapeutically active substances to the specific cell compartments, in particular, the nucleus, bypassing the endosomal pathway [10].

Liposomes or micelles formed by amphiphilic compounds are commonly used as nanoparticle drug carriers. In this regard, poly(ethylene oxide) [11], poly(L-lactide) [12], poly(epsilon-caprolactone) [13], poly(lactic-co-glycolic acid) [14] and poly-N-vinyl-2-pyrrolidone (PVP) [15–21] have gained widespread acceptance. Intranuclear drug delivery represents a particular challenge, since transport into a nucleus is strictly controlled by nuclear pore complexes [22]. Traditionally, viruses [10,23–26], liposomes [10,26] and complexes with proteins, interacting specifically with the nuclear membrane, for example, nucleoplasmin [27] and the TAT penetrating peptide [28], are used to deliver pharmaceutically active substances and genetic material to cell nuclei. In particular, DNA viruses, which are naturally adapted for penetration into a nucleus, such as the adenovirus [23,24] and the simian vacuolating virus 40 [25], have been reported to deliver genetic material to a cell nucleus. Although the use of DNA viruses ensures high translocation efficiency, significant risks associated with viruses limit the applicability of this approach for therapeutic purposes [10,26]. On the other hand, the use of nonviral methods for the delivery of pharmacologically active substances is in general associated with carrier lability [10,26].

Nanocarriers based on amphiphilic poly-N-vinyl-2-pyrrolidones are of particular interest for drug delivery, some of them being already approved for clinical studies [29]. We have previously shown that amphiphilic derivatives of poly-N-vinylpyrrolidone can be used both to increase liposomal membrane stability [30] and construct self-assembled nanocarriers for various low-molecular [31] and high-molecular [32] model hydrophobic drugs. More importantly, our studies have shown that the amphiphilic PVPs and nano-scaled PVP drug carriers are biocompatible since they possess low toxicity [33], do not influence blood components and their properties [34] and decrease side toxicity of model pharmacologically active substances [35].

In this study, we introduce the use of an amphiphilic poly-N-vinyl-2-pyrrolidone containing a thiooctadecyl end-group (PVP-OD) as an adaptable nanocarrier of biologically active compounds. The PVP-OD was synthesized via the radical polymerization of N-vinyl-2-pyrrolidone using azobisisobutyronitrile (AIBN) to initiate the polymerization and octadecyl mercaptan as the chain transfer agent. Curcumin was selected as model hydrophobic pharmaceutically active substance primarily due to its fluorescence properties and lack of toxicity, but also because of its established antioxidant [36–39], anti-inflammatory [38,40] and anticancer activity [41], which have drawn significant interest to the compound, in particular, in a nanodispersed form. We demonstrate that we can tailor the size of the PVP-OD nanoparticles by simple means and that, depending on the size of these nanoparticles, the delivery system exhibits two distinct mechanisms of cell penetration via endocytosis and by diffusion through the cell membrane. In the latter case, curcumin was observed in the nuclei of the U87 glioblastoma cells and CRL 2429 fibroblasts, which generally opens the possibility for intranuclear drug delivery. The possibility of using sub-100 nm carriers formed by amphiphilic polymers to deliver therapeutic compounds to cell nuclei presents a fundamental new result.

Materials & methods

Materials

N-vinylpyrrolidone, 2,2′-Azobisisobutyronitrile, 1,4-dioxane were obtained from Acros (Geel, Belgium). Octadecyl mercaptan, curcumin, 1,6-diphenyl-1,3,5-hexatriene (DPH), dynasore (3-Hydroxy-naphthalene-2-carboxylic acid (3,4-dihydroxy-benzylidene)-hydrazide), Wortmannin from *Penicillium funiculosum* ((1S, 6bR, 9aS, 11R, 11bR)-1-(methoxymethyl)-9a, 11b-dimethyl-3, 6, 9-trioxo-3, 6, 6b, 7, 8, 9, 9a, 10, 11, 11b -decahydro-1H-furo[4, 3, 2-de]indeno[4, 5-h]isochromen-11-yl acetate) and the Hoechst 33258 (4-[6-(4-Methyl-1-piperazinyl)[2,6'-bi-1H-benzimidazol]-2'-yl]phenol trihydrochloride) were purchased from Sigma-Aldrich (MO, USA). All chemicals were used without further purification unless otherwise specified. All solvents and components of buffer solutions were of analytical grade and were used as received. A Milli-Q Plus Water Purification System (Merck, Darmstadt, Germany) was used for preparation of deionized water, which was used throughout the experiments. ^{1}H NMR and ^{13}C NMR spectra of the products were obtained using an Avance Bruker DPX-300 NMR (Bruker, MA, USA) spectrometer in deuterated dimethyl sulfoxide. Chemical shifts were reported as δ in units of p.p.m. referenced to the residue solvent peak. IR spectra were obtained on a Nicolet-380 spectrometer (Thermo Fisher Scientific, MA, USA) in KBr tablets. Fluorescence spectra were obtained with a Hitachi 650-10S spectrofluorometer (Hitachi, Tokyo, Japan).

Synthesis & characterization of PVP-OD

Thiooctadecyl poly-N-vinyl-2-pyrrolidone (PVP-OD) was synthesized and characterized as has been reported earlier [42] (see Supplementary Data for full detail).

The critical micelle concentration was determined by fluorescence spectroscopy using DPH as the fluorescent probe at excitation wavelength λ_{ex} = 366 nm and emission wavelength λ_{em} = 433 nm [43].

Preparation & characterization of PVP-OD colloidal particles

Two different preparation procedures, based on emulsification and ultrasonic suspension were employed to prepare curcumin-loaded PVP-OD nanocarriers. In the suspension approach, the amphiphilic PVP-OD was initially dispersed in water (0.1 g/ml) while curcumin was dissolved in acetone (0.01 g/ml). Equal volumes of the polymer and the curcumin solution were then mixed under ultrasonic excitation (CV33 Sonics Vibracel, Sonics & Materials, CT, USA) in an ice bath. The samples were then rapidly frozen with liquid nitrogen and lyophilized.

To produce particles using the emulsion approach, a solution of curcumin in chloroform was initially prepared (0.01 g/ml). The curcumin solution was added dropwise to a dispersion of the amphiphilic PVP-OD in water (0.1 g/ml) under ultrasonic treatment in an ice bath. The chloroform was then evaporated under vacuum in a rotary evaporator (IKA RV10 + HB10 Digital, IKA Works, NC, USA) and the resulting solution frozen in liquid nitrogen and lyophilized. It should be noted that under these conditions no insoluble residues were observed, indicating that we operate below the loading capacity of PVP-OD nanocarriers. Determination of curcumin loading degree in PVP-OD nanoparticles is reported in the Supplementary Data.

In order to remove the fraction of small-diameter particles, the solution of curcumin-loaded nanocarriers via the suspension approach was filtered using an Amicon centrifugal filter device (Merck Millipore) with a molecular weight cut-off of 30 kDa according to the manufacturer's guidelines.

For subsequent experiments, the lyophilized particle powders were dispersed in deionized water (0.02 g/ml). In all cases, particle size distribution was determined by nanoparticle tracking analysis (NTA) using a Nanosight LM10 (Malvern, UK) instrument equipped with a 642 nm laser and a camera. The original particle suspension was diluted with deionized water to a concentration of 1 mg/ml prior to measurements; the temperature was continuously monitored by a thermocouple and was typically about 25°C. Briefly, during the measurement, the solution was illuminated with a laser beam, and the motion of all particles within the field of view of an optical microscope was recorded with a video camera and tracked by the instrument software. Based on the obtained Brownian motion trajectories, the hydrodynamic diameter of each particle was evaluated and the particle size distribution was plotted. Each sample was measured for 160 s at 30 frames per second; the measurements were performed in triplicate and averaged. The obtained number distributions were analyzed to obtain the mean size and standard deviation (SD).

The morphology of the polymeric nanoparticles was analyzed by transmission electron microscopy (JEOL JEM-2100, Jeol, Tokyo, Japan) at accelerating voltage of 120 kV. A minute quantity of the PVP-OD nanoparticle suspension was deposited on copper grid covered with 0.2% polyvinyl formal. Excess liquid was removed by filter paper and the grids were dried at room temperature.

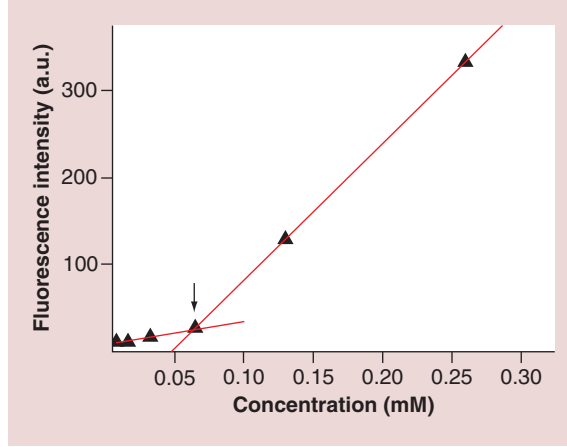

Figure 1. Fluorescence emission intensity of DPH (λ_{ex} = 366 nm/λ_{em} = 433 nm) as a function of the concentration of the PVP-OD block copolymer in water at 25°C. The arrow indicates the onset of the formation of DPH-loaded PVP-OD nanocarriers.
a.u.: Arbitrary units.

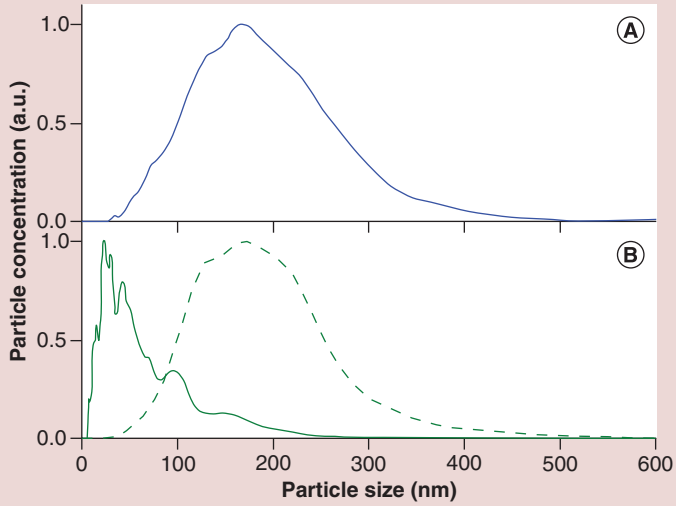

Figure 2. Size distributions (number distribution) for emulsion- and suspension-produced nanocarriers obtained using nanoparticle tracking analysis (NTA). The solid lines show size distributions (number distribution) of the curcumin-loaded PVP-OD micelles obtained by **(A)** the emulsion approach and **(B)** by the suspension approach. The dashed line shows a typical distribution obtained after filtration of the nanocarriers produced by the suspension method using a 30 kDa molecular weight cut-off centrifugal filter. The curves are normalized to the peak value. a.u.: Arbitrary units.

ζ-potential of the obtained carriers is determined using Zetasizer Nano Z&S (Malvern Instruments Ltd, Malvern, UK). The measurements were carried out at 25°C and pH 7.4 (phosphate-buffered saline [PBS]) using disposable folded capillary cells. The measurements were performed in triplicate.

Atomic force microscopy (AFM) visualization of the nanocarriers was performed using a Multimode Nanoscope IIIA (Bruker) operating in a tapping mode. Soft OMCL-AC240TS (Olympus, Tokyo, Japan) and HA-NC (ScanSens, Hamburg, Germany) cantilevers with nominal spring constants of 2 and 3.5 N/m, respectively, were used for the measurements. Briefly, freshly cleaved muscovite mica pieces, ca. 1 × 1 cm^2, were treated with (3-aminopropyl)trimethoxysilane (Sigma-Aldrich) in vapor phase (see [44] for more detail) to create a positively charged surface. Next, a solution of curcumin-loaded nanocarriers was incubated on top of the functionalized mica for 5–10 min. Then the mica plates were rinsed with deionized water, dried under nitrogen stream and imaged in AFM. The obtained images were processed using built-in Nanoscope as well as WSxM v.5 [45] software.

Cell cultures & cell uptake studies

The human glioblastoma-derived cell line (U87, ATCC no. HTB-14) and primary human fibroblasts (ATCC no. CRL 2429) were cultured in growth medium consisting of Dulbecco's modified eagle medium (F12), basal medium supplemented with 100 U/ml penicillin, 10 mg/ml streptomycin and 10% fetal bovine serum. The cells were maintained in culture flasks (75 cm^2, Greiner Bio One, Germany) in a standard incubator at 5% CO_2 and 37°C.

For the cell uptake studies, the cells were seeded into 96-well polystyrene plates at a density of ca. 5000 cells/cm^2. For each cell type, three different experimental conditions were accessed: a negative control, a dynasore-treated group and a wortmannine-treated group. Dynasore blocks dynamin-dependent endocytosis by scission of endocytic vesicles [46], while wortmannin is an inhibitor of the receptor-mediated endocytosis of the cellular PI3-K [47]. 24 h after seeding, the cells were washed with PBS and then preincubated for 15 min with the Hoechst 33258 fluorescent DNA-binding dye dissolved in the cell medium at a ratio of 1:1000 and subsequently washed with the medium [48]. The cells were then exposed to the inhibitor solutions (12.5 µl dynasore in 1 ml of medium [80 mM] and 0.11 µl of wortmannin in 1 ml of medium [100 nM]) at 37°C for 30 min. Wells without inhibitor were incubated with growth media for the same period of time. Finally, the cells were treated with 150 µl of curcumin-loaded PVP-OD nanocarriers (0.13 mg/ml in medium) for 5 min for the nanocarriers stemming from the suspension approach and 10 min for nanocarriers stemming from the emulsion approach. To monitor the uptake process, the cells were

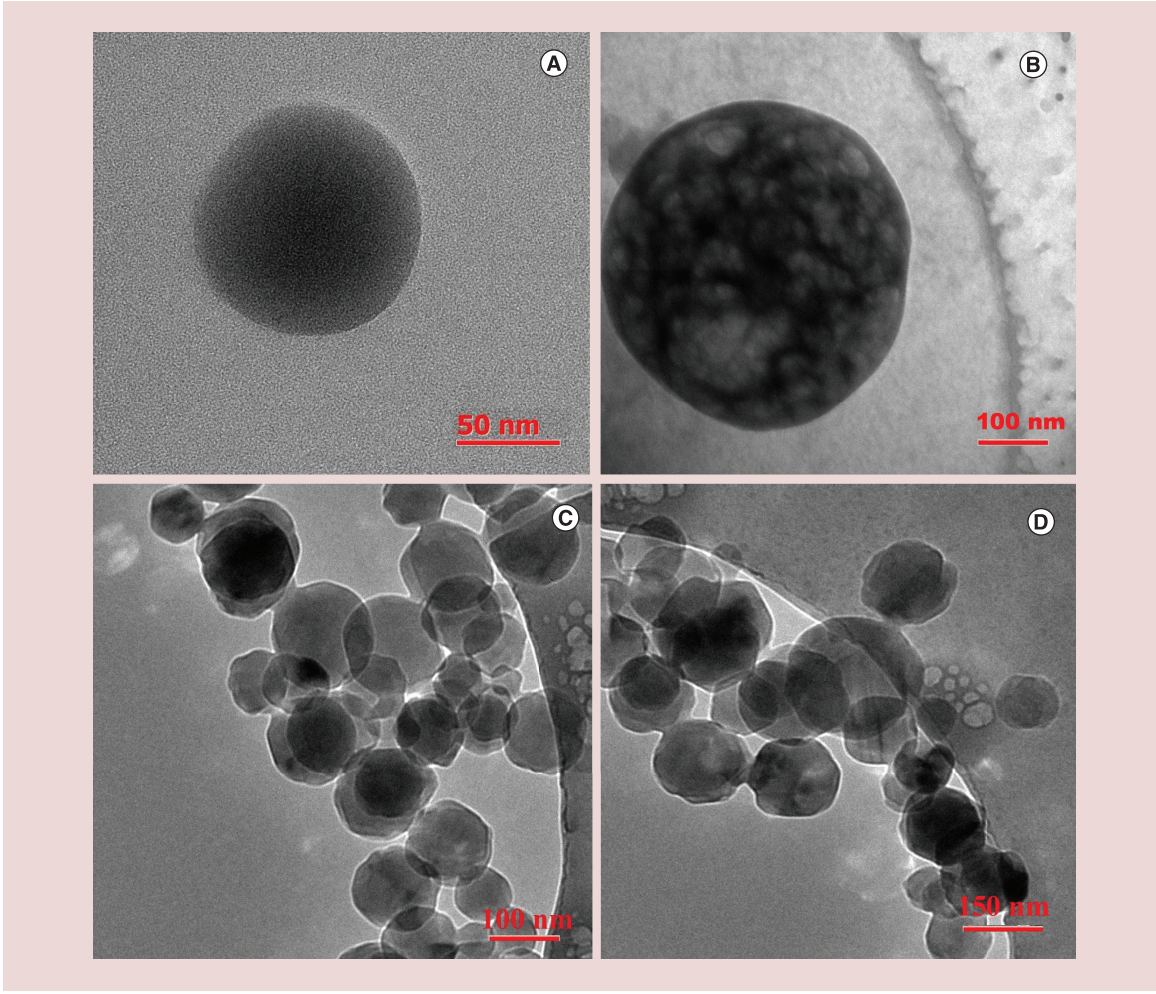

Figure 3. Transmission electron microscopy micrographs of curcumin-loaded PVP-OD nanoparticles. Micrographs **(A & C)** illustrate nanoparticles produced by the suspension method, while **(B & D)** nanoparticles produced by the emulsion method.

washed three-times with PBS and then imaged using an Axio Observer.Z1 inverted microscope (Zeiss, Oberkochen, Germany).

Cellular uptake of curcumin was quantified as relative fluorescence intensity at the curcumin emission wavelength per cell, determined by the ratio of the number of bright pixels above a certain threshold (corresponding to the background) in the curcumin fluorescence channel (excitation 493 nm and emission 517 nm) to that in the Hoechst channel (excitation 353 nm and emission 465 nm) using Zen Lite image-processing software (Zeiss, Oberkochen, Germany) and MATLAB (MathWorks, MA, USA) [49].

The distribution of curcumin with respect to cell nuclei was analyzed by calculating fluorophore colocalization [50] in the curcumin and Hoechst fluorescence channels. The calculations were performed using coloc2 plugin to ImageJ processing software [51].

Results & discussion

The amphiphilic thiooctadecyl terminated poly-N-vinyl-2-pyrrolidone (PVP-OD) used in this study was synthesized by radical polymerization of N-vinyl-2-pyrrolidone using AIBN as radical chain initiator and octadecyl mercaptan as chain transfer agent according to previous reports [42,52]. Nuclear magnetic resonance and IR spectroscopy were employed to fully characterize the produced polymer (see Supplementary Data for full synthesis and characterization).

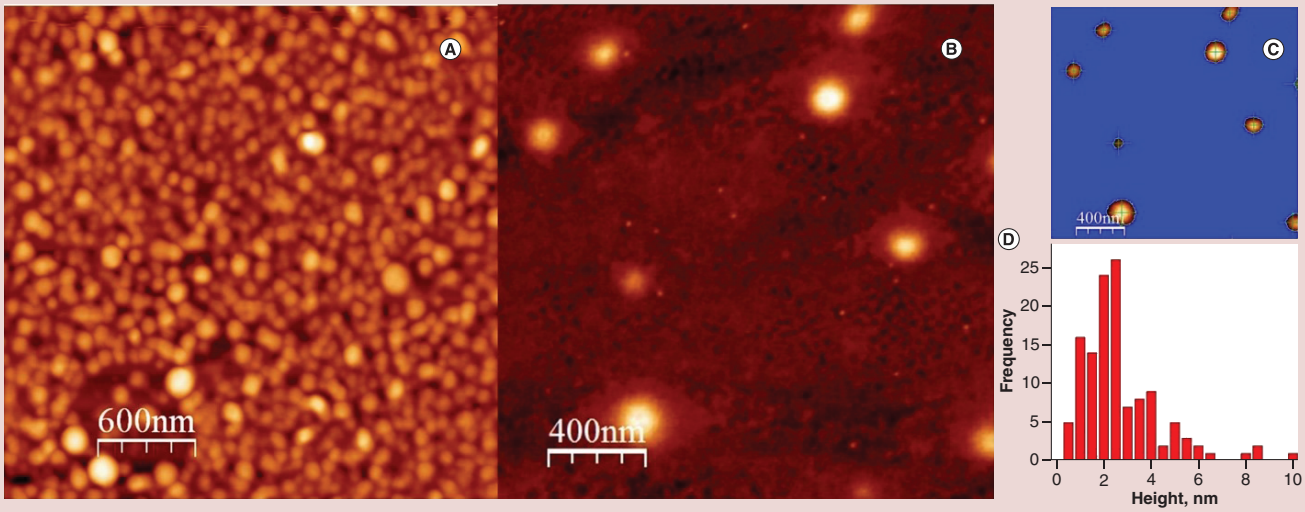

Figure 4. Atomic force microscopy (AFM) visualization and analysis of nanocarriers. Curcumin-loaded nanocarriers produced by the suspension method are deposited on mica surface and visualized with AFM **(A)**. To evaluate the size distribution of the produced nanocarriers, deposition with a lower coverage was obtained **(B)**, where the particles are well separated and can be identified and measured using WSxM flooding procedure **(C)**. The resulting size distribution obtained after processing of ten different low-coverage images is shown **(D)**.

Based on the chemical structure of PVP-OD we can assume that the radicals produced by the thermal decomposition of AIBN react with the octadecyl mercaptan to form thiooctadecyl radicals which in turn can react with the monomer N-vinyl-2-pyrrolidone causing its polymerization. In view of the high activity of mercaptans with respect to radicals, the termination of the resulting polymer chain is expected to occur almost exclusively by transfer. End-group analysis [42] revealed a low number average molecular weight, equal to 6050 Da for the PVP-OD. The formation of low molecular weight polymers is consistent with the high activity of octadecyl mercaptan in the chain transfer. The presence of the thiooctadecyl end-group is further confirmed by the ability of the synthesized compound to form self-assembled nanoparticles at concentrations above 0.065 mmol/l in aqueous media in the presence of DPH which was used in the present study as a fluorescent hydrophobic marker (Figure 1).

The PVP-OD nanocarriers were found to successfully solubilize the highly hydrophobic curcumin which was used as a model pharmaceutically active component in the present study. Two loading techniques commonly used in literature – the emulsification and the ultrasonically-assisted suspension – were employed to prepare nanocarriers and found to lead to different size distributions of the nanocarriers shown as solid lines in Figure 2A and B. NTA measurements revealed that the curcumin-loaded nanocarriers prepared using the emulsion approach exhibit a broad, rather symmetric hydrodynamic diameter distribution with a median at 170 nm, mean diameter of 200 nm, SD of 90 nm and practically no sub-50 nm particles present (Figure 2A). On the other hand, the suspension method led to a strongly asymmetric size distribution peaked at 30 nm with a mean diameter of 73 nm, SD of 56 nm and majority of particles in sub-50 nm range (Figure 2B, solid lines). In both cases, according to measurements, the obtained particles were slightly negatively charged with ζ-potential of -4.0 ± 0.3 mV. Transmission electron microscopy pictures of PVP-OD curcumin-loaded nanoparticles show that their shape is close to spherical with a diameter below 100 nm for the suspension method and about 200–300 nm for the emulsion (Figure 3). This agrees with the particle size distributions obtained using nanoparticle tracking analysis.

The size distribution of curcumin-loaded nanocarriers was further visualized and evaluated using AFM. A representative topographic image showing nanocarriers deposited on mica at high density is shown in Figure 4A. To evaluate the size distribution, a lower density deposition was made and ten different images similar to Figure 4B were analyzed. Each image was processed using the flooding procedure of WSxM to determine the center of each micelle and its height, as illustrated in Figure 4C. This yielded a distribution shown in Figure 4D with a mean height of 2.7 nm and SD of 0.9 nm. It can be seen that the micelles collapse when deposited on the surface and the hydrodynamic diameter of the nanocarriers determined by NTA is significantly larger than the size of collapsed

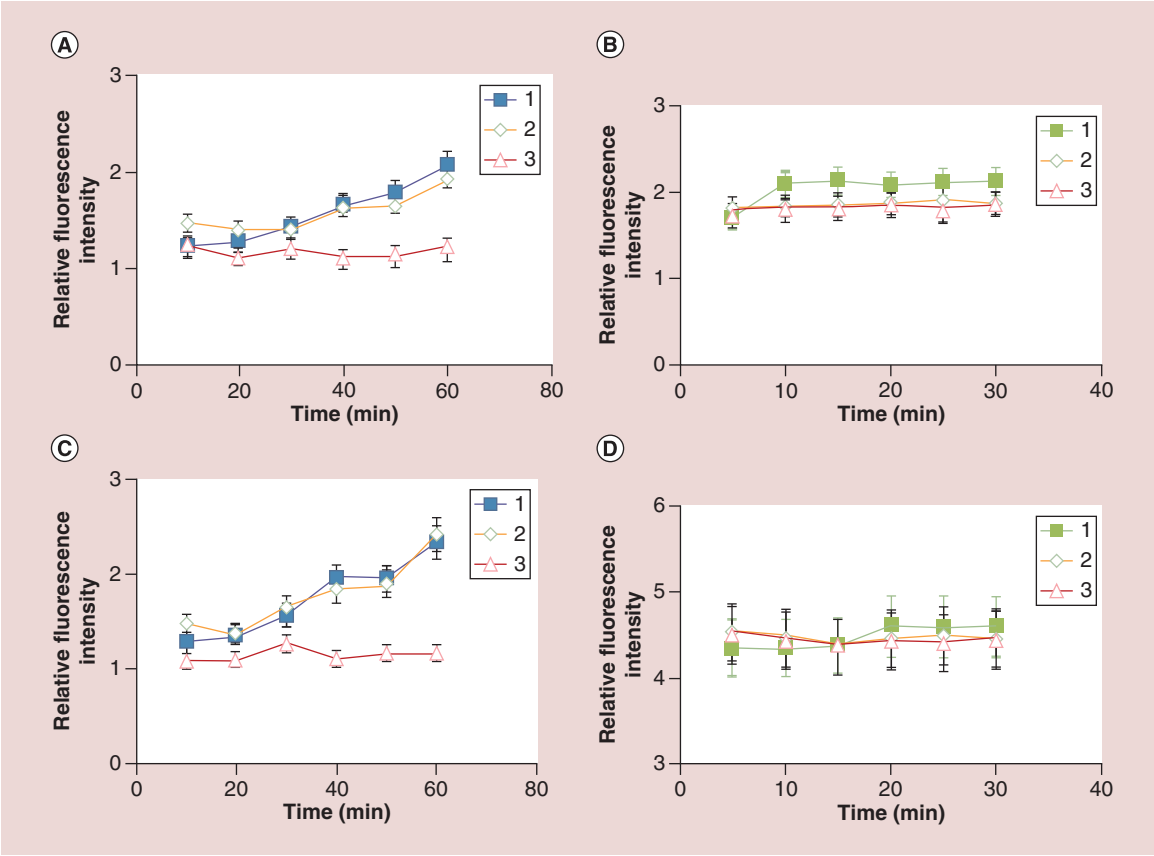

Figure 5. Kinetics of *in vitro* uptake of curcumin-loaded PVP-OD nanocarriers by U87 (A & B) and CRL 2429 (C & D) cells. Panels **(A)** and **(C)** show the uptake of the emulsion-produced nanocarriers; panels **(B)** and **(D)** correspond to the nanocarriers produced via the ultrasonic-dispersion route. In all panels – 1: uptake without endocytosis inhibitors; 2: uptake in the presence of wortmannin; and 3: uptake in the presence of dynasore. Standard error is shown for each data point.

micelles visualized by AFM. This can also explain high penetrative ability of the nanocarriers observed in cell studies.

The curcumin-loaded PVP-OD micelles were used for the *in vitro* studies of nanoparticle uptake by U87 glioblastoma and CRL 2429 fibroblast cells. When the nanocarriers produced by the emulsion method were introduced into the cell cultures under study in the absence of endocytosis inhibitors, a slow increase in the relative fluorescence intensity of curcumin with time was observed whereas in the presence of dynasore, it remained constant (Figure 5). Since the nanoparticle carriers used in the present study did not possess any specific receptor-targeting moieties, no inhibitory effect was expected in the presence of wortmannin, which blocks the receptor-mediated endocytosis. The blocking effect of dynasore was clearly visible in both fibroblast and glioblastoma cultures (Figure 5A & C).

These observations clearly indicate that the uptake of curcumin-loaded PVP-OD nanocarriers produced by the emulsion approach mainly proceeds through dynamin-dependent mechanisms of endocytosis. This is also confirmed by the presence of a significant amount of curcumin-labelled endosomes in U87 (Figure 6A) and CRL 2429 cells (Figure 6B). It should be noted that the obtained micrographs indicate the presence of the curcumin-loaded PVP-OD nanocarriers in the interior cytosolic compartments of the U87 (Figure 6A) and CRL 2429 (Figure 6B) cells, while the nuclei show no emission in the curcumin channel indicating that they are not permeable by these nanocarriers. Colocalization analysis of curcumin and the nucleic stain (Hoechst channel) shows that the two dyes are located in different compartments without any significant overlap: as shown by the 2D intensity histograms (right column in Figure 6), bright pixels in the curcumin channel correspond to dark ones in

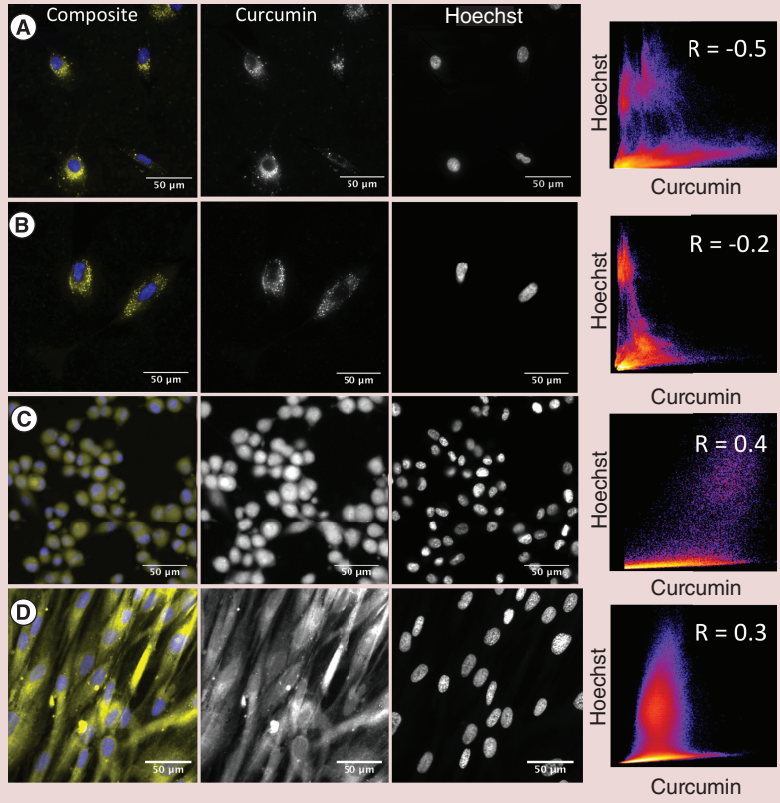

Figure 6. Uptake of curcumin-loaded nanocarriers by U87 and CRL 2429 cells. Fluorescence images showing: U87 **(A & C)** and CRL 2429 **(B & D)** cells after incubation with curcumin-loaded PVP-OD micelles produced by the emulsion **(A & B)** and suspension **(C & D)** methods. 2D-histograms show colocalization of fluorophores in curcumin (517 nm, yellow) and Hoechst (465 nm, blue) fluorescence channels and the respective Pearson correlation coefficient R.

the Hoechst channel and vice versa leading to a specific rectangular shape of the histogram. This confirms that the emulsion-produced curcumin nanocarriers are mainly localized in the cytoplasm and cannot penetrate the nuclei.

Similarly, both the U87 and CRL 2429 cell lines were shown to uptake the smaller diameter nanoparticles prepared via the suspension approach. However, as shown in Figure 5, the presence of endocytosis inhibitors do not affect the nanocarrier uptake kinetics. Extremely fast uptake was observed with the maximum relative fluorescence reached within 5 min for both the reference samples and those exposed to dynasore and wortmannin. Furthermore, in this case, curcumin was observed throughout the cellular compartments, for example, that a particle subfraction was also present in the nuclei (Figure 6C & D). Notably, no significant intensity change in the curcumin fluorescence channel is observed at the nuclei location as compared with the emulsion-produced nanocarriers (cf. panels A & C, and B & D in Figure 6). This conclusion is supported by colocalization analysis showing a partial overlap of curcumin and nucleic stain fluorescence channels for both CRL 2429 and U87 cell lines. While curcumin is present in some cell compartment with no nucleic stain (lower branch in the 2D intensity histogram), there is also a significant population of pixels with high intensity of both curcumin and nucleic stain.

Further evidence for different internalization of the suspension and emulsion produced nanocarriers in CRL 2429 and U87 cell lines, is provided by 3D fluorescence images consisting of 50 z-stacked layers (Figure 7). The figure shows the image plane at mid height together with two vertical cross-sections passing through the nucleus of one of the imaged cells. It can be clearly seen that in the case of emulsion-produced nanocarriers, curcumin is not present inside the nuclei of CRL 2429 and U87 cells, while in the case of suspension-produced nanocarriers, curcumin patches are observed inside the nuclei in all the cross-sections.

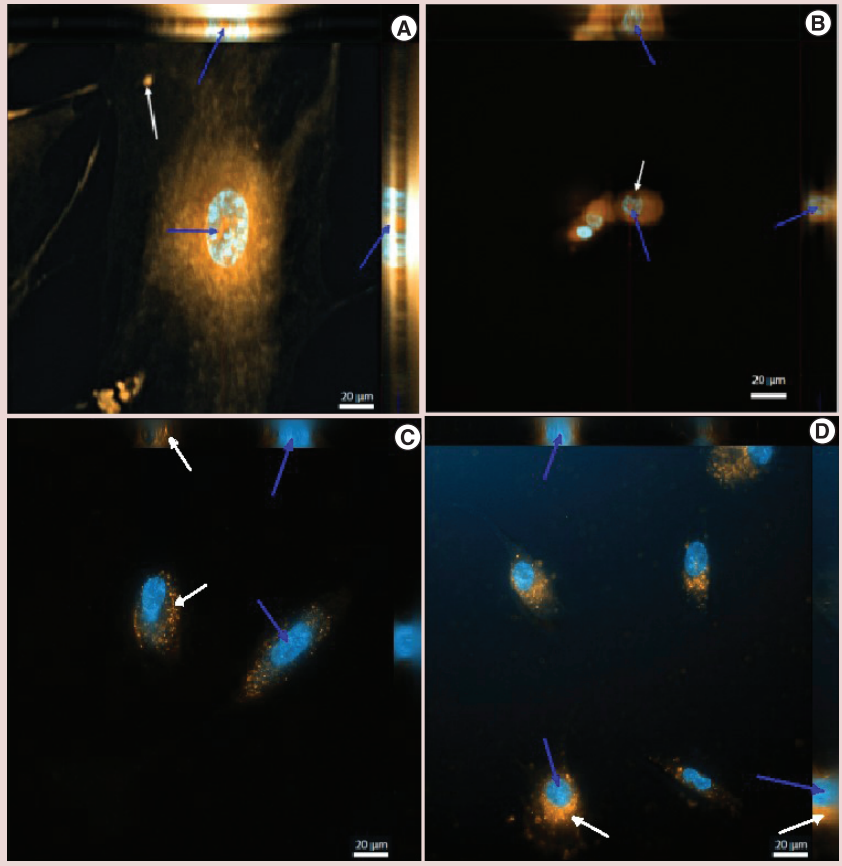

Figure 7. 3D fluorescence images show CRL 2429 (A & C) and U87 (B & D) cells incubated with a 1 mg/ml solution of curcumin-loaded PVP-OD nanocarriers for 30 min. Images in panels **(A)** and **(B)** show cells treated with nanocarriers produced by the suspension method, panels **(C)** and **(D)** correspond to nanocarriers obtained by the emulsion method. The images were obtained by superimposing the Hoechst (465 nm, blue) and curcumin (517 nm, orange) fluorescence channels, with exposure times of 100 and 700 ms, respectively. Stripes on the right side and above the images show the vertical cross-section passing through the nucleus of one of the cells. The blue and white arrows indicate the respective intranuclear and extranuclear compartments in the main panel and cross-sections.

The ability of the sub-100 nm nanocarriers to deliver curcumin into cell nuclei provides the possibility of fast and efficient intranuclear delivery of pharmaceutically active substances bypassing enzymatic degradation in the lysosomes.

To confirm the assumption that it is the small-size fraction of nanocarriers that is responsible for fast dynamin-independent curcumin uptake to all cellular compartments, we removed the small-size fraction of the nanocarriers using an Amicon centrifugal filter device with 30 kDa molecular weight cut-off. As can be seen in Figure 2 (cf. solid and dashed lines in panel B), nanoparticles with the average diameters below 50 nm were efficiently removed. Similar to the size distribution obtained by the emulsion method, we obtained a mean size of 200 nm, median of 170 nm and SD of 80 nm. Cell studies performed with the filtered fraction showed that it acts in the same way as emulsion-prepared nanocarriers (Figure 8) and its delivery was efficiently stopped by preincubating cells in dynasore (data not shown).

The interaction of the PVP-OD curcumin nanocarriers with average diameters greater than 50 nm obtained via filtration with CRL 2429 fibroblast and U87 glioblastoma cell cultures in the absence of endocytosis inhibitors was subsequently studied. Figure 8 clearly demonstrates that these larger nanocarriers are no longer able to enter the nuclei of the cell.

It is well known that the size of nanocarriers strongly affects cellular uptake [53]. However, this phenomenon is considered to be primarily related to the features of the endocytic pathway, in particular the optimal bending curva-

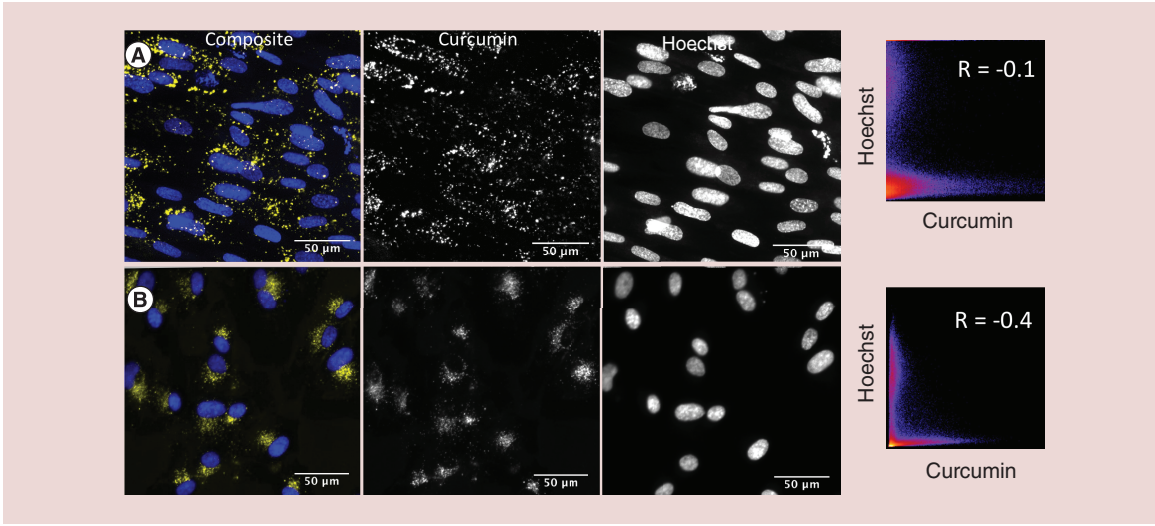

Figure 8. Uptake of filtered curcumin-loaded nanocarriers. Fluorescence images showing CRL 2429 **(A)** and U87 **(B)** cells after incubation with curcumin-loaded PVP-OD nanocarriers produced by the suspension method and then filtered using 30 molecular weight cut-off centrifugal filter units. From left to right: Curcumin (517 nm, yellow) and Hoechst (465 nm, blue) fluorescence channels, the composite image and 2D histograms showing colocalization of fluorophores in the channels and the respective Pearson correlation coefficient.

ture of the membrane, required to drive the membrane-wrapping process and the formation of an invagination [53]. This process is also affected by the number of available targeting moieties on the surface of the nanoparticle interacting with receptors on the cell surface. However, in our case the uptake process is not affected by the presence of uptake inhibitors and the nanocarriers do not possess any specific targeting moieties. This implies a nonendocytic pathway for the cellular uptake of nanocarriers. This is a relatively understudied field where the main focus has been the application of cell-penetrating peptides as functional moieties [54]. It has been found that certain cell-penetrating peptides are capable of inducing nonendocytic uptake of their cargo through transient destabilization of a membrane and formation of a pore suitable for transportation of a relatively large cargo [55,56]. On the other hand, modeling studies have shown that amphiphilic nanoparticles (so-called Janus particles) are also capable of direct translocation through the membrane [57] and pore formation [58] facilitating uptake of further particles. Evidently, such mechanisms pave the way for particle penetration not only through the cell membrane but also into other intracellular compartments, including the nucleus. Interestingly, such indiscriminate penetration of small polymeric nanocarriers throughout cell compartments has been observed in [59], however, the authors have not performed inhibition studies, and hence it remains unclear whether the uptake process was endocytic or not. Although further studies are necessary to identify the exact uptake mechanism, the fact that polymeric nanocarriers with average diameters less than 50 nm exhibit a different cell penetration mechanism opens the exciting possibility of delivering pharmaceutically active substances to various cell compartments including the cell nucleus.

Conclusion

It was shown that the amphiphilic PVP-OD is capable of forming nanocarriers in aqueous media at concentrations exceeding 0.065 mmol/l, as well as of solubilizing highly hydrophobic compounds such as curcumin. Two of the most commonly used methods for drug loading – emulsification and ultrasonic dispersion – were successfully employed and found to lead to the formation of carriers with different particle size distributions and, more importantly, a distinctively different biological effect. Specifically, the emulsion-produced nanocarriers were found to lack sub-100 nm particles, which were abundant in the dispersion-produced nanocarriers. Using the U87 glioblastoma and CRL 2429 fibroblast cells as model systems, we found that nanocarriers produced via the emulsion route penetrate cells by endocytic mechanisms. On the other hand, sub-100 nm nanocarriers produced by ultrasonic dispersion were found to cross cellular membranes via nonendocytic mechanisms with a very fast kinetics. They were observed to deliver the model hydrophobic drug throughout all cellular compartments including the nucleus. This opens the intriguing possibility to deliver pharmaceutically active substances into cell nuclei by merely tailoring the size of polymeric carriers.

Summary points

- Amphiphilic thiooctadecyl-terminated poly-N-vinyl-2-pyrrolidone (PVP-OD) was synthesized by radical polymerization and nuclear magnetic resonance and IR spectroscopy were employed to fully characterize the produced polymer.
- It was demonstrated that PVP-OD is capable of emulsifying hydrophobic compounds at low concentration.
- Two commonly used drug-loading methods – emulsification and ultrasonic dispersion – were successfully applied to form nanocarriers loaded with curcumin-model pharmaceutically active hydrophobic compound used in the study.
- It was shown that these two loading methods lead to different size distribution, where ultrasonic dispersion contains large fraction of sub-100 nm particles.
- Uptake studies employing glioblastoma and fibroblasts as well as two uptake inhibitors – dynasore and wortmannine – were carried out.
- It was found that the nanocarriers produced by the emulsification method penetrate the cells via dynamin-dependent endocytosis and cannot enter the nucleus, while ultrasonic dispersion penetrates cells by diffusion and delivers hydrophobic drug throughout all cell compartments including the nucleus.
- Elimination of sub-100 nm fraction from the suspension-produced nanocarriers also removes the ability to penetrate cell nuclei.

Supplementary data

To view the supplementary data that accompany this paper please visit the journal website at: www.futuremedicine.com/doi/suppl/10.2217/nnm-2017-0311.

Financial & competing interests disclosure

The research was partially funded by ERA.NET RUS PLUS program (ID#169 – NABUCO). K Velonia acknowledges the Special Account for Research Funds of the University of Crete for funding. AL Luss and PP Kulikov gratefully acknowledge scholarships from Danish Ministry of Higher Education and Science granted within the Cultural Exchange program between Russia and Denmark, which facilitated their research stay at Aalborg University. L Gurevich acknowledges travel support by Det Obelske Familiefond. L Gurevich also acknowledges A Bombin, P Patel, J Svirelis and M Babu for sharing their data. The authors have no other relevant affiliations or financial involvement with any organization or entity with a financial interest in or financial conflict with the subject matter or materials discussed in the manuscript apart from those disclosed.

No writing assistance was utilized in the production of this manuscript.

Ethical conduct of research

The authors state that they have obtained appropriate institutional review board approval or have followed the principles outlined in the Declaration of Helsinki for all human or animal experimental investigations. In addition, for investigations involving human subjects, informed consent has been obtained from the participants involved.

References

Papers of special note have been highlighted as: • of interest; •• of considerable interest

1. Wilczewska AZ, Niemirowicz K, Markiewicz KH *et al.* Nanoparticles as drug delivery systems. *Pharmacol. Rep.* 64, 1020–1037 (2012).
2. Qiu Liping, Chen Tao, Ocsoy Ismail *et al.* A cell-targeted, size-photocontrollable, nuclear-uptake nanodrug delivery system for drug-resistant cancer therapy. *Nano Lett.* 15, 457–463 (2015).
3. Sahay G, Alakhova DY, Kabanov AV. Endocytosis of nanomedicines. *J. Control. Rel.* 145(3), 182–195 (2010).

•• **Excellent review of endocytosis in application to drug delivery.**

4. Kou L, Sun J, Zhai Y, He Z. The endocytosis and intracellular fate of nanomedicines: implication for rational design. *Asian J. Pharmac. Sci.* 8(1), 1–10 (2013).
5. Kindl H. Lysosomes and peroxisomes. In: *Cytology and cell Physiology (4th Edition).* Bourne GH (Ed.). Academic Press, Inc., San Diego, CA, USA, 325–355 (1987).

6. Engin AB, Neagu M, Golokhvast K, Tsatsakis A. Nanoparticles and endothelium: an update on the toxicological interactions. *Farmacia* 63(6), 792–804 (2016).
7. Engin AB, Nikitovic D, Neagu M *et al.* Mechanistic understanding of nanoparticles' interactions with extracellular matrix: the cell and immune system. *Part. Fibre Toxicol.* 14(1), 22–38 (2017).
8. Neagu M, Piperigkou Z, Karamanou K *et al.* Protein bio-corona: critical issue in immune nanotoxicology. *Arch. Toxicol.* 91(3), 1031–1048 (2017).
9. Piperigkou Z, Karamanou K, Engin AB *et al.* Emerging aspects of nanotoxicology in health and disease: from agriculture and food sector to cancer therapeutics. *Food Chem. Toxicol.* 91, 42–57 (2016).
10. Sakhrani NM, Padh H. Organelle targeting: third level of drug targeting. *Drug Des. Devel. Ther.* 7, 585–599 (2013).
11. Zhang T, Yu YY, Li D *et al.* Synthesis and properties of a novel methoxy poly(ethylene glycol)-modified galactosylated chitosan derivative. *J. Mater. Sci. Mater. Med.* 20(3), 673–680 (2009).
12. Hossein Panahi F, Peighambardoust SJ, Davaran S, Salehi R. Development and characterization of PLA-mPEG copolymer containing iron nanoparticle-coated carbon nanotubes for controlled delivery of docetaxel. *Polymer* 117, 117–131 (2017).
13. Aliabadi HM, Mahmud A, Sharifabadi AD, Lavasanifar A. Micelles of methoxy poly(ethylene oxide)-b-poly(e-caprolactone) as vehicles for the solubilization and controlled delivery of cyclosporine A. *J. Control Release* 104 (2), 301–311 (2005).
14. Takeuchi I, Tomoda K, Hamano A, Makino K. Effects of physicochemical properties of poly(lactide-co-glycolide) on drug release behavior of hydrophobic drug-loaded nanoparticles. *Colloids Surfaces A Physicochem. Eng. Asp.* 520, 771–778 (2017).
15. Kaneda Y, Tsutsumi Y, Yoshioka Y *et al.* The use of PVP as a polymeric carrier to improve the plasma half-life of drugs. *Biomaterials* 25(16), 3259–3266 (2004).
16. Alifragis J, Rizos A, Tsatsakis AM, Tzatzarakis M, Shtilman MI. New polymeric systems with controlled release action: a light-scattering investigation. *J. Non-Cryst. Solids* 307, 882–886 (2002).
17. Baritaki S, Krambovitis E, Alifragis J, Rizos AK, Shtilman M, Tsatsakis AM. Immunoreactivity and light scattering studies of polyvinylpyrrolidone polymeric derivatives. *J. Non-Cryst. Solids* 307, 898–904 (2002).
18. Rizos AK, Tsikalis I, Tsatsakis AM, Shtilman MI. Characterization of amphiphilic poly-*N*-vinylpyrrolidone derivatives by dynamic light scattering. *J. Non-Cryst. Solids* 352, 5055–5059 (2006).
19. Kuskov AN, Shtilman MI, Goryachaya AV *et al.* Self-assembling nanoscaled drug delivery systems composed of amphiphilic poly-N-vinylpyrrolidones. *J. Non-Cryst. Solids* 353, 3969–3975 (2007).
20. Kuskov AN, Voskresenskaya AA, Goryachaya AV, Artyukhov AA, Shtilman MI, Tsatsakis AM. Preparation and characterization of amphiphilic poly-N-vinylpyrrolidone nanoparticles containing indomethacin. *J. Mater. Sci. Mater. Med.* 21(5), 1521–1530 (2010).
21. Papadimitriou S, Bikiaris D. Dissolution rate enhancement of the poorly water-soluble drug tibolone using PVP, SiO2, and their nanocomposites as appropriate drug carriers. *Drug Dev. Ind. Pharm.* 35(9), 1128–1138 (2009).
22. Pouton CW, Wagstaff KM, Roth DM, Moseley GW, Jans DA. Targeted delivery to the nucleus. *Adv. Drug Deliv. Rev.* 59, 698–717 (2007).
23. Ran L, Tan X, Li Y *et al.* Delivery of oncolytic adenovirus into the nucleus of tumorigenic cells by tumor microparticles for virotherapy. *Biomaterials* 89, 56–66 (2016).
24. Strunze S, Trotman LC, Boucke K, Greber UF. Nuclear targeting of adenovirus type 2 requires CRM1-mediated nuclear export. *Mol. Biol. Cell* 16(6), 2999–3009 (2005).
25. Nabi IR, Le PU. Caveolae/raft-dependent endocytosis. *J. Cell Biol.* 161(4), 673–677 (2003).
26. Mali S. Delivery systems for gene therapy. *Indian J. Hum. Genet.* 19(1), 3–8 (2013).
27. Robbins J, Dilworth SM, Laskey RA, Dingwall C. Two interdependent basic domains in nucleoplasmin nuclear targeting sequence: identification of a class of bipartite nuclear targeting sequence. *Cell* 64(3), 615–623 (1991).
28. Torchilin VP, Levchenko TS, Rammohan R, Volodina N, Papahadjopoulos-Sternberg B, D'Souza GG. Cell transfection *in vitro* and *in vivo* with nontoxic TAT peptide–liposome–DNA complexes. *Proc. Natl Acad. Sci. USA* 100(4), 1972–1977 (2003).
29. Giodini L, Re FL, Campagnol D *et al.* Nanocarriers in cancer clinical practice: a pharmacokinetic issue. *Nanomedicine* 13(2), 583–599 (2017).
30. Yamskov IA, Kuskov AN, Babievsky KK *et al.* Novel liposomal forms of antifungal antibiotics modified by amphiphilic polymers. *Appl. Biochem. Microbiol.* 44(6), 624–628 (2008).
31. Kuskov AN, Voskresenskaya AA, Goryachaya AV *et al.* Amphiphilic poly-N-vinylpyrrolidone nanoparticles as carriers for non-steroidal anti-inflammatory drugs: characterization and *in vitro* controlled release of indomethacin. *Int. J. Mol. Med.* 26(1), 85–94 (2010).
32. Kuskov AN, Shtilman MI, Villemson AL *et al.* Amphiphilic poly-N-vinylpyrrolidone nanocarriers with incorporated model proteins. *J. Phys. Condens. Matter.* 19(20), 5139–5150 (2007).
33. Kuskov AN, Kulikov PP, Shtilman MI *et al.* Amphiphilic poly-N-vynilpyrrolidone nanoparticles: cytotoxicity and acute toxicity study. *Food Chem. Toxicol.* 96, 273–279 (2016).

34. Villemson AL, Kuskov AN, Shtilman MI *et al.* Interaction of polymer aggregates based on stearoyl-poly-N-vinylpyrrolidone with blood components. *Biochemistry (Mosc.)* 69(6), 621–628 (2004).
35. Kuskov AN, Kulikov PP, Goryachaya AV *et al.* Amphiphilic poly-N-vinylpyrrolidone nanoparticles as carriers for non-steroidal, anti-inflammatory drugs: *in vitro* cytotoxicity and *in vivo* acute toxicity study. *Nanomedicine* 13(3), 1021–1030 (2017).
36. Margină D, Olaru OT, Ilie M *et al.* Assessment of the potential health benefits of certain total extracts from *Vitis vinifera*, *Aesculus hyppocastanum* and *Curcuma longa*. *Exp. Ther. Med.* 10(5), 1681–1688 (2015).
37. Agarwal R, Goel SK, Behari JR. Detoxification and antioxidant effects of curcumin in rats experimentally exposed to mercury. *J. Appl. Toxicol.* 30(5), 457–468 (2010).
38. Menon VP, Sudheer AR. Antioxidant and anti-inflammatory properties of curcumin. *Adv. Exp. Med. Biol.* 595, 105–125 (2007).
39. Tataringa G, Stan C, Mircea C, Jitareanu A, Zbancioc AM. Antioxidant evaluation of some coumarin derivatives. *Farmacia* 64(4), 533–538 (2016).
40. dos Santos Filho EX, Ávila PHM, Bastos CCC *et al.* Curcuminoids from *Curcuma longa*. reduced intestinal mucositis induced by 5-fluorouracil in mice: bioadhesive, proliferative, anti-inflammatory and antioxidant effects. *Toxicol. Rep.* 3, 55–62 (2016).
41. Siddiqui RA, Harvey KA, Walker C *et al.* Characterization of synergistic anti-cancer effects of docosahexaenoic acid and curcumin on DMBA-induced mammary tumorigenesis in mice. *BMC Cancer* 13, 418–433 (2013).
42. Kulikov PP, Kuskov AN, Goryachaya AV, Luss AN, Shtilman MI. Amphiphilic poly-N-vinyl-2-pyrrolidone: synthesis, properties, nanoparticles. *Polymer Science Series D* 10(3), 264–268 (2017).
43. Priev A, Zalipsky S, Cohen R, Barenholz Y. Determination of critical micelle concentration of lipopolymers and other amphiphiles: comparison of sound velocity and fluorescent measurements. *Langmuir* 18(3), 612–617 (2002).
44. Fojan P, Gurevich L. Atomic force microscopy study of the interactions of indolicidin with model membranes and DNA. In: *Antimicrobial Peptides: Methods and Protocols.* Hansen PR (Ed.). Springer, NY, USA, 201–215 (2017).
45. Horcas I, Fernández R, Gómez-Rodríguez JM, Colchero J, Gómez-Herrero J, Baro AM. WSXM: a software for scanning probe microscopy and a tool for nanotechnology. *Rev. Sci. Instrum.* 78(1), 13705 (2007).
46. Macia E, Ehrlich M, Massol R, Boucrot E, Brunner C, Kirchhausen T. Dynasore, a cell-permeable inhibitor of dynamin. *Dev. Cell.* 10(6), 839–850 (2006).
47. Arcaro A, Wymann MP. Wortmannin is a potent phosphatidylinositol 3-kinase inhibitor: the role of phosphatidylinositol 3,4,5-trisphosphate in neutrophil responses. *Biochem. J.* 296(2), 297–301 (1993).
48. Daxhelet GA, Coene MM, Hoet PP, Cocito CG. Spectrofluorometry of dyes with DNAs of different base composition and conformation. *Anal. Biochem.* 179(2), 401–403 (1989).
49. Unciti-Broceta JD, Cano-Cortés V, Altea-Manzano P, Pernagallo S, Díaz-Mochón JJ, Sánchez-Martín RM. Number of nanoparticles per cell through a spectrophotometric method – a key parameter to assess nanoparticle-based cellular assays. *Sci. Rep.* 5, 10091 (2015).
50. Dunn KW, Kamocka MM, McDonald JH. Practical guide to evaluating colocalization in biological microscopy. *Am. J. Physiol. Cell Physiol.* 300(4), C723–C742 (2011).
51. Schindelin J, Arganda-Carreras I, Frise E. "Fiji: an open-source platform for biological-image analysis". *Nat. Methods* 9(7), 676–682 (2012).
52. Gangolli S. *The Dictionary of Substances and Their Effects (2nd Edition).* Royal Society Chemistry, Cambridge, UK, 6 (1999).
53. Han H. The effect of nanoparticle size on *in vivo* pharmacokinetics and cellular interaction. *Nanomedicine* 11, 673–692 (2016).

• **Interesting study on the effect of nanoparticle size on its *in vivo* pharmacokinetics.**

54. Verma A, Stellacci F. Effect of surface properties on nanoparticle–cell interactions. *Small* 6(1), 12–21 (2010).

• **Interesting study on the effect of surface properties on nanoparticle interactions with cells.**

55. Madani F, Lindberg S, Langel U *et al.* Mechanisms of cellular uptake of cell-penetrating peptides. *J. Biophys.* 2011, 414729 (2011).
56. Heitz F, Morris MC, Divita G. Twenty years of cell-penetrating peptides: from molecular mechanisms to therapeutics. *Br. J. Pharmacol.* 157(2), 195–206 (2009).
57. Ding H-M, Ma Y-Q. Interactions between Janus particles and membranes. *Nanoscale* 4, 1116–1122 (2012).
58. Alexeev A, Uspal WE, Balazs AC. Harnessing Janus nanoparticles to create controllable pores in membranes. *ACS Nano* 2(6), 1117–1122 (2008).
59. Savic R, Luo L, Eisenberg A, Maysinger D. Micellar nanocontainers distribute to defined cytoplasmic organelles. *Science* 300(5619), 615–618 (2003).

•• **Interesting colocalization study, showing that details of a passive nanocarrier can strongly affect the intracellular distribution of its load.**